Melanocortin 1 Receptor–Targeted α-Particle Therapy for Metastatic Uveal Melanoma

Narges K. Tafreshi*[1], Christopher J. Tichacek*[1–3], Darpan N. Pandya*[4], Michael L. Doligalski*[1], Mikalai M. Budzevich[5], HyunJoo Kil[6], Nikunj B. Bhatt[4], Nancy D. Kock[7], Jane L. Messina[8–10], Epifanio E. Ruiz[5], Nella C. Delva[1], Adam Weaver[11], William R. Gibbons[11], David C. Boulware[12], Nikhil I. Khushalani[13], Ghassan El-Haddad[14], Pierre L. Triozzi[15], Eduardo G. Moros[1–3,10], Mark L. McLaughlin[6], Thaddeus J. Wadas[4], and David L. Morse[1,3,5,10]

[1]Department of Cancer Physiology, H. Lee Moffitt Cancer Center and Research Institute, Tampa, Florida; [2]Department of Radiation Oncology, H. Lee Moffitt Cancer Center and Research Institute, Tampa, Florida; [3]Department of Physics, University of South Florida, Tampa, Florida; [4]Department of Cancer Biology, Wake Forest University Health Sciences, Winston-Salem, North Carolina; [5]Small Animal Imaging Laboratory, H. Lee Moffitt Cancer Center and Research Institute, Tampa, Florida; [6]Department of Pharmaceutical Sciences, Health Sciences Center, West Virginia University, and Modulation Therapeutics Inc., Morgantown, West Virginia; [7]Section on Comparative Medicine, Department of Pathology, Wake Forest University Health Sciences, Winston-Salem, North Carolina; [8]Departments of Anatomic Pathology and Cutaneous Pathology, H. Lee Moffitt Cancer Center and Research Institute, Tampa, Florida; [9]Department of Dermatology, University of South Florida, Tampa, Florida; [10]Department of Oncologic Sciences, University of South Florida, Tampa, Florida; [11]Division of Research Integrity and Compliance, University of South Florida, Tampa, Florida; [12]Biostatistics Core Facility, H. Lee Moffitt Cancer Center and Research Institute, Tampa, Florida; [13]Department of Cutaneous Oncology, H. Lee Moffitt Cancer Center and Research Institute, Tampa, Florida; [14]Departments of Diagnostic Imaging and Interventional Radiology, H. Lee Moffitt Cancer Center and Research Institute, Tampa, Florida; and [15]Department of Hematology and Oncology, Wake Forest University Health Sciences, Winston-Salem, North Carolina

New effective therapies are greatly needed for metastatic uveal melanoma, which has a very poor prognosis with a median survival of less than 1 y. The melanocortin 1 receptor (MC1R) is expressed in 94% of uveal melanoma metastases, and a MC1R-specific ligand (MC1RL) with high affinity and selectivity for MC1R was previously developed. **Methods:** The ^{225}Ac-DOTA-MC1RL conjugate was synthesized in high radiochemical yield and purity and was tested in vitro for biostability and for MC1R-specific cytotoxicity in uveal melanoma cells, and the lanthanum-DOTA-MC1RL analog was tested for binding affinity. Non–tumor-bearing BALB/c mice were tested for maximum tolerated dose and biodistribution. Severe combined immunodeficient mice bearing uveal melanoma tumors or engineered MC1R-positive and -negative tumors were studied for biodistribution and efficacy. Radiation dosimetry was calculated using mouse biodistribution data and blood clearance kinetics from Sprague–Dawley rat data. **Results:** High biostability, MC1R-specific cytotoxicity, and high binding affinity were observed. Limiting toxicities were not observed at even the highest administered activities. Pharmacokinetics and biodistribution studies revealed rapid blood clearance (<15 min), renal and hepatobillary excretion, MC1R-specific tumor uptake, and minimal retention in other normal tissues. Radiation dosimetry calculations determined pharmacokinetics parameters and absorbed α-emission dosages from ^{225}Ac and its daughters. Efficacy studies demonstrated significantly prolonged survival and decreased metastasis burden after a single administration of ^{225}Ac-DOTA-MC1RL in treated mice relative to controls. **Conclusion:** These results suggest significant potential for the clinical translation of ^{225}Ac-DOTA-MC1RL as a novel therapy for metastatic uveal melanoma.

Key Words: melanocortin 1 receptor; ^{225}Ac alpha therapy; uveal melanoma; mouse model

J Nucl Med 2019; 60:1124–1133
DOI: 10.2967/jnumed.118.217240

Uveal melanoma is the most common primary intraocular malignancy and differs from the more common cutaneous melanoma in terms of risk factors, primary treatment, anatomic spread, molecular changes, and response to systemic therapy (*1,2*). Patients who develop uveal melanoma metastases, primarily in the liver, have a very poor prognosis with a median survival of about 1 y. Because uveal melanomas have different characteristic mutations from cutaneous melanomas, targeted therapies that have been effective for the latter, such as BRAF, are not indicated for the former (*3*). Immune checkpoint inhibition therapies that are successful in cutaneous melanoma have had poor efficacy in ocular melanoma, with fewer than 10% of patients responding and with rapid recurrence (*3*).

The melanocortin 1 receptor (MC1R) is highly expressed in uveal melanoma metastases (*4*). MC1R is a member of a family of 5 G-protein–coupled melanocortin receptors, 4 of which bind melanocyte-stimulating hormone (MSH) and related ligands (MC1R, 3R, 4R, and 5R) (*5*). Unlike the other members of this G-protein family, MC1R is not expressed in most normal human tissues (*6*), lessening concern for therapy-related toxicity. Although expression is found in the brain (*7*) and normal melanocytes (*8*), this is not a major concern because conjugates can be designed to not cross

Received Jul. 6, 2018; revision accepted Dec. 20, 2018.
For correspondence contact: David L. Morse, Moffit Cancer Center and Research Institute, 12902 Magnolia Dr., SRB 24000B, Tampa, FL 33612.
E-mail: david.morse@moffitt.org
*Contributed equally to this work.
Published online Feb. 7, 2019.

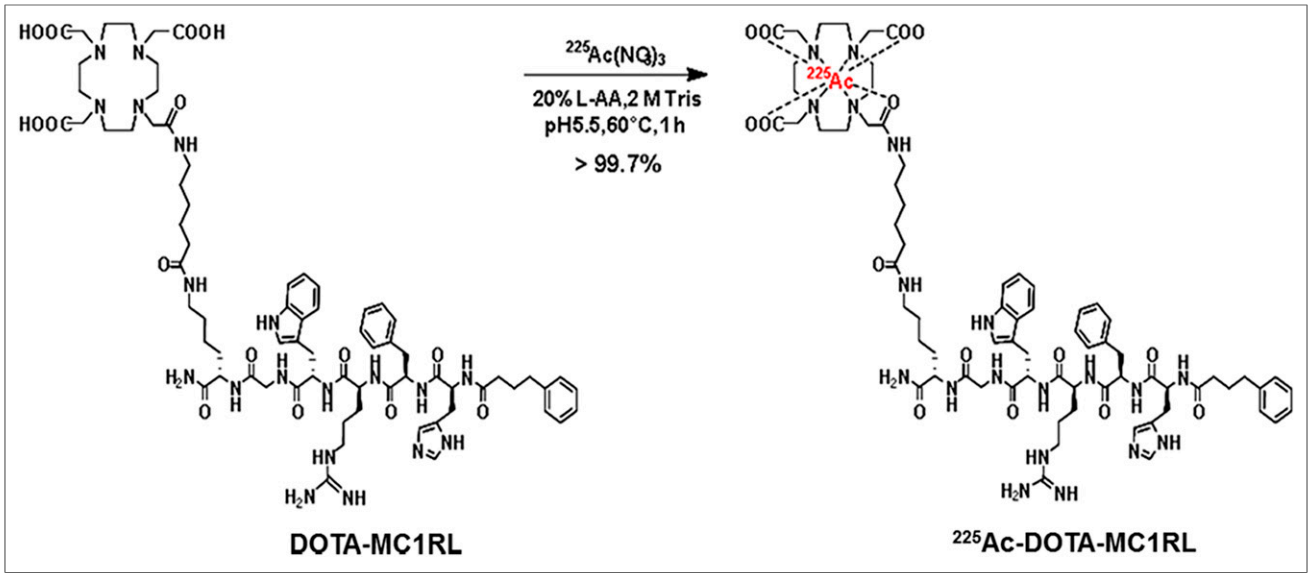

FIGURE 1. Radiochemical synthesis of ^{225}Ac-DOTA-MC1RL.

the blood–brain barrier and, in the most severe cases of melanocyte loss, the most serious symptom is vitiligo (*9*). MC1R expression has been reported on activated monocytes, macrophages, and dendritic cells derived from monocytes (*10*). This is also not a significant concern since the population of activated monocytes and macrophages can be replenished within days and lymphoid dendritic cells, which do not express MC1R, will not be depleted. MC1R is highly polymorphic (*11*), but the wild-type frequency is about 50% (*8*) and the most common mutations occur with a frequency of 21.5% in cytoplasmic domains, 19.7% in transmembrane domains, and 0% in the extracellular domain (*11*). Hence, most patients will have an MC1R isoform that is suitable for ligand binding. An MC1R-specific ligand (MC1RL) and conjugates were previously developed with high specificity (>200 fold) and affinity (0.2–0.4 nM inhibition constant) for MC1R (*12,13*). A fluorescent-dye conjugate was rapidly internalized by MC1R-expressing tumor cells, does not cross the blood–brain barrier, and is rapidly cleared from circulation (*7*).

Herein is reported the preclinical development and testing of a novel MC1R-targeted radiopharmaceutical, ^{225}Ac-DOTA-MC1RL, for targeted α-particle therapy (TAT) (*14,15*) of uveal melanoma. α-particle emissions consist of dicationic helium nuclei (He^{2+}) that have high linear-energy transfer and a short mean free path of only a few cell diameters (<100 μm) in tissue (*16*). ^{225}Ac is an α-particle–emitting radionuclide that has a 10-d half-life (*17*), 4 α-emissions in its decay chain, and high (28 MeV) total energy release (*18*).

MATERIALS AND METHODS

Compound Synthesis and Loading with Lanthanide

MC1RL (*13*) was synthesized according to a conventional N^{α}-fluorenylmethyloxycarbonyl (Fmoc) peptide synthesis strategy, except the Fmoc-Lys(Alloc)-OH was coupled to allow orthogonal alloc deprotection of the linker on the ε-amino group of the lysine after the linear peptide synthesis. The alloc group is removed, and Fmoc-aminohexanoic acid linker and tri-t-butyl-1,4,7,10-tetraazacyclododecane-1,4,7,10-tetraacetate (DOTA; TCI Chemicals) were coupled sequentially using *O*-(1H-6-chlorobenzotriazole-1-yl)-1,1,3,3-tetramethyluronium hexafluorophosphate activation. The DOTA-MC1RL peptide was cleaved from the resin with a cocktail of trifluoroacetic acid (Chem-Impex International), water, and triisopropylsilane (Sigma-Aldrich) (95:2.5:2.5, v/v), precipitated in cold diethyl ether, pelleted/decanted, and lyophilized. The crude white powder was purified by reverse-phase high-performance liquid chromatography (Agilent) and characterized by both matrix-assisted laser desorption/ionization time-of-flight mass spectroscopy (JEOL USA Inc.) and analytic high-performance liquid chromatography. A scrambled peptide ligand (DOTA–substance P [SP]) was synthesized by changing the order of amino acids (sequence: 4-phenylbutyric acid-Trp-Gly-His-Arg-(D)-Phe-Lys(aminohexanoic acid-DOTA)-$CONH_2$). The europium–diethylenetriaminepentaacetic acid (DTPA)–MC1RL was synthesized as described before (*19*) except that MC1RL was used as the binding ligand (Supplemental Figs. 1A–1C; supplemental materials are available at http://jnm.snmjournals.org). Competition binding assays were performed as previously described using the europium-DTPA-NDPα-MSH ligand. The europium-DTPA-MC1RL binding affinity was determined using saturation binding assays. To determine MC1RL binding affinity for murine MC1RL, saturation binding assays were performed using the europium-DTPA-MC1RL and B16-F10 murine melanoma cells with high expression of murine MC1R (*12*).

Cell Culture and Characterization

Uveal melanoma cell lines were acquired (OCM1, OCM3, and OCM8 from June Kan-Mitchel, University of Southern California;

TABLE 1
In Vitro Serum Stability of ^{225}Ac-DOTA-MC1RL

	% intact	
Day	Thin-layer chromatography scanner	γ-counter
0	100	100
2	97.3 ± 0.5	96.9 ± 0.4
4	95.6 ± 1.1	95.1 ± 0.8
6	93.5 ± 0.8	93.2 ± 1.3
8	91.4 ± 1.2	91.0 ± 0.9
10	90.2 ± 0.7	89.9 ± 1.3

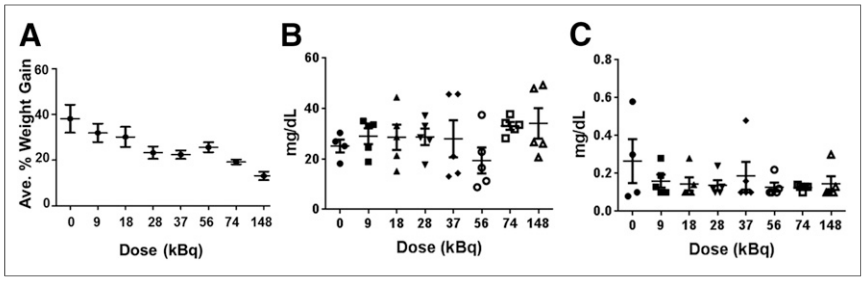

FIGURE 2. MTD study for non–tumor-bearing mice: percentage weight gain (A), blood urea nitrogen (B), and blood creatinine (C).

OMM1 from Gregorius P. Luyten, University Hospital at Rotterdam; and MEL270, MEL290, and OMM2.3 from Timothy Murray, Bascom Palmer Eye Institute) and grown in RPMI medium, 10% fetal bovine serum, a 100 units/mL concentration of penicillin, a 100 mg/mL concentration of streptomycin, 1% 200 mM L-glutamine, 1% 100 mM sodium pyruvate, 1% minimal essential medium essential vitamin mixture (×100), 1% nonessential amino acid mixture (×100), and 1% 1 M (4-(2-hydroxyethyl)-1-piperazineethanesulfonic acid) in 5% CO_2 at 37°C. A375, A375/MC1R human cutaneous melanoma cells, and Hek293/MC1R cells were obtained and grown as before (*12,20*). Cells were authenticated per American Type Culture Collection guidelines (*21*), monitored for original morphology, and tested for *Mycoplasma* (MycoAlert kit; Lonza), and only passage numbers of less than 25 cells were used. MC1R expression and receptor number were determined as previously described (*12,13*) except that europium-DTPA-MC1RL was used for saturation binding. Cytotoxicity was determined as described in Supplemental Figure 2.

Radiochemical Synthesis and Characterization

DOTA-MC1RL or DOTA-SP (10 μg/10 μL of water), $^{225}Ac(NO_3)_3$ (3.4 MBq), 90 μL of water, and 10 μL of 20% L-ascorbic acid were added to a 1.5-mL tube followed by pH adjustment to 5.5–6 (1 M Tris buffer;10–12 μL) and incubation at 60°C for 1 h (Fig. 1). Specific activity was calculated using a standard method (*22*). Radiochemical purity was assessed 24 h after collection by a γ-counter, and in vitro serum stability was determined by adding 50 μL of ^{225}Ac-DOTA-MC1RL (2,072 kBq) to 1 mL of human serum (n = 4), incubated at 37°C for 10 d, and quantified at multiple time points by thin-layer chromatography and γ-counting using established methods (*23*).

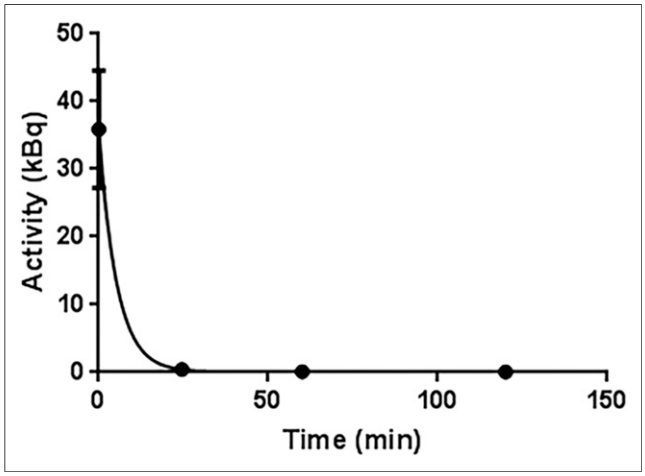

FIGURE 3. Plot of rat blood clearance: exponential decay nonlinear regression line fit of ^{225}Ac α-activity in rat blood over time, after intravenous administration of ^{225}Ac-DOTA-MC1RL (n = 4 rats).

Animal Studies

All protocols were approved (University of South Florida Institutional Animal Care and Use Committee protocol IS00000805 and Wake Forest University Health Sciences Institutional Animal Care and Use Committee protocol A11-144). Male and female animals were used. Sprague–Dawley rats, 10–12 wk old and weighing 200–250 g, were purchased with jugular vein catheters installed (Charles River). Nontumor studies used BALB/c mice (10–12 wk old, 18–22 g; Charles River). Severe combined immunodeficient (SCID) mice (6–8 wk old, 15–20 g; Charles River) were used for xenografting cell lines. Tail vein catheters were used for agent administration to mice.

For xenografting, 10×10^6 cells in 80 μL of phosphate-buffered saline and 20 μL of Matrigel (phenol red–free; Corning) were injected subcutaneously into the flank. Tumor volumes were determined by caliper using the following formulas: volume = (length × width^2)/2 for A375 and A375/MC1R, and volume = (length × width × height)/2 for MEL270 tumors, which were initially flat with a gradual shift to a rounded shape.

Histology and Immunohistochemistry

Excised tissues were prepared for histology, hematoxylin and eosin staining, MC1R immunohistochemistry staining, and slide scanning as previously described (*12*). Metastasis burden was determined using images of 3 sections (25%, 50%, and 75%) through each liver and lung. Metastasis area was determined by segmentation using intensity and size threshold classifiers on the triple-red channel (Visiopharm software, version 6.7.0.2590). Total tissue area was determined with an intensity threshold classifier on the immunohistochemistry intensity channel, and the percentage metastasis was calculated.

To quantify MC1R expression in tumors, images from serial hematoxylin and eosin and immunohistochemistry sections were analyzed using Visiopharm, version 2017.7. Each serial section pair (hematoxylin and eosin and immunohistochemistry) was aligned using the tissue align module, and viable tumor was segmented by thresholding the hematoxylin channel. A multithreshold-marker-area analysis was then performed within the viable tumor region on each immunohistochemistry image. Each pixel was categorized as negative, weak, moderate, or strong on the basis of thresholds set by a pathologist, and the percentages of each category were normalized by total area of interest.

Maximum Tolerated Dose (MTD)

The MTD study was performed as previously described (*23*).

Measurement of Activity

Because α-particles from ^{225}Ac cannot be directly measured in tissue because of the short mean free path (*18*), ^{225}Ac α-activities were estimated using measurements of related γ-emissions. For the initial MTD study, syringes were prepared with a range of activities as determined by the γ-counter (Wallac 1470 Wizard; Perkin-Elmer). For subsequent studies, a dose calibrator (Atomlab 500; BioDex) was used to prefill syringes with 148 kBq ± 10% (per Appendix E of the BioDex manual) of ^{225}Ac-conjugate activity. Activities were measured for 2 min using dial number 38.2 as recommended by Biodex. Activities of ^{225}Ac, and the ^{221}Fr and ^{213}Bi daughter products (*18*), were measured by acquiring isomeric γ-spectra (Supplemental Fig. 3) before administration using a 4π well-type wipe-test γ-counter (Atomlab 500). Activities (^{225}Ac) were calculated using factors for γ-ray abundance per α-decay using calibration parameters and correction coefficients from Appendices A and E of the instrument manual. A full energy window

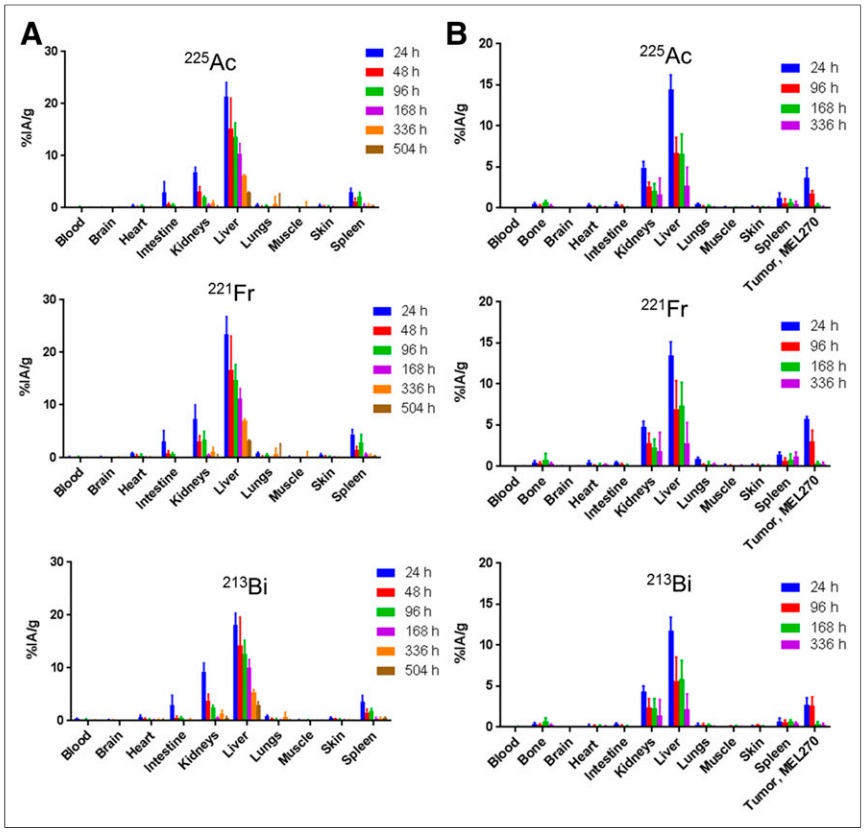

FIGURE 4. Biodistribution of ^{225}Ac-DOTA-MC1RL: ^{225}Ac, ^{221}Fr, and ^{213}Bi activities in tissues from non–tumor-bearing BALB/c mice (n = 6 per time point) (A) and SCID mice bearing MEL270 human uveal melanoma tumors (n = 5 per time point) (B).

(0–800 keV) was used for spectra acquisition that included γ-counts from ^{225}Ac (99.8-keV peak, 1% abundance) and 2 γ-emitting daughters, ^{221}Fr (218.1-keV peak, 11.4% abundance) and ^{213}Bi (440.5-keV peak, 25.9% abundance) (*24*). The α-activities were determined by fitting each peak with a multigaussian fit and integrating to determine the net number of counts while incorporating the acquisition time. Spectra were acquired at least 24 h after radiosynthesis or tissue rendering, ensuring that ^{225}Ac and daughters were in secular equilibrium (*25*). Activity remaining in the syringe and catheter after injection was calculated and subtracted to determine net administered activity.

Blood Pharmacokinetics

Sprague–Dawley rats were weighed before injection with radioactivity and injected with 148 kBq (±10%) of ^{225}Ac-DOTA-MC1RL in the syringe. Serial blood draws (45 μL) were taken from 5 min to 24 h after injection. ^{225}Ac α-activity was calculated as described above. Data were fitted using an exponential decay nonlinear regression.

Biodistribution

Non–tumor-bearing BALB/c mice, or SCID mice bearing MEL270 xenografts (160–650 mm^3) or A375 and A375/MC1R bilateral xenografts (189–1,680 mm^3), were intravenously administered 148 kBq (±10%) of ^{225}Ac α-activity in the syringe. Tissues were rendered and weighed at multiple time-points between 24 h and 3 wk after injection. For each tissue, ^{225}Ac, ^{221}Fr, and ^{213}Bi α-activities were calculated as described above and reported as percentage injected activity per gram (%IA/g).

Radiation Dosimetry

Biodistribution data for the different tissues were fitted using an exponential decay nonlinear regression, and dosimetry calculations were performed for ^{225}Ac, ^{221}Fr, ^{217}At, ^{213}Bi, and ^{213}Po using the generalized internal dosimetry schema of the MIRD Committee for α-particle emitters (*26,27*). The β^- decay branching ratio for ^{217}At to ^{217}Rn is only 0.01%; therefore, it was assumed that all decays of ^{217}At were by α-emission to ^{213}Bi. The branching ratios for decay of ^{213}Bi to ^{213}Po (98%) or ^{209}Tl (2%) were included in the calculation. Because of the relatively low linear-energy transfer and the small dimensions of the target tissues, the β^- emissions from ^{217}At, ^{213}Bi, ^{209}Tl, and ^{209}Pb were assumed negligible and were not included in the calculations (*28*). The following assumptions were made: uniform distribution of activity in the tissue volume; no α-particles escaping from the source tissue due to the short range; and electron and photon contributions that were negligible compared with α-particle energy deposition (*28*). It was also assumed that α-particles from ^{221}Fr (4.9-min half-life), ^{217}At (32.2-ms half-life), ^{213}Bi (46-min half-life), and ^{213}Po (4.2-μs half-life) were deposited in the same location as ^{225}Ac (10-d half-life) because of the relatively shorter half-lives of these daughter isotopes. Although ^{217}At and ^{213}Po do not have detectable γ-emissions, under the assumption that the decay chain had reached secular equilibrium, the accumulated activity of these 2 daughters would equal that of ^{221}Fr

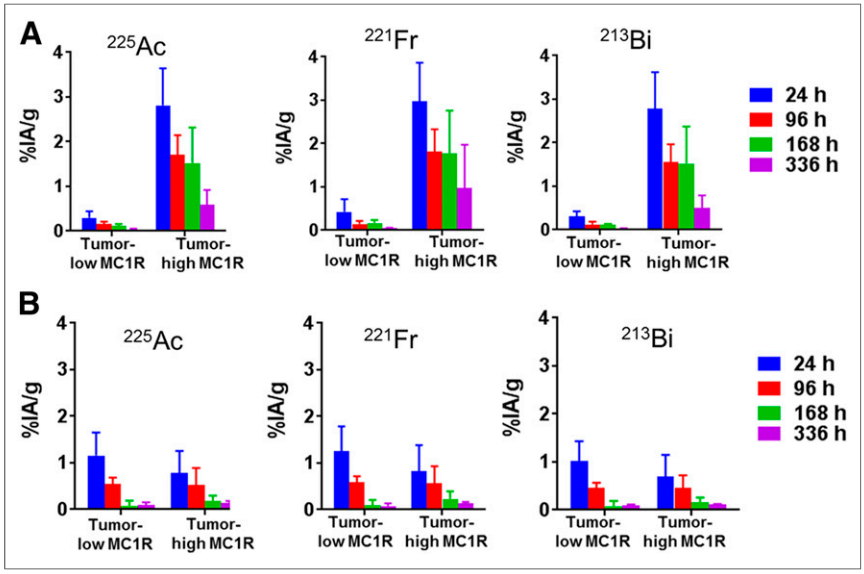

FIGURE 5. Biodistribution of ^{225}Ac-DOTA-MC1RL (A) and ^{225}Ac-DOTA-SP (B) in bilateral A375 and A375/MC1R tumors (n = 5 per time point).

TABLE 2
Radiation Dosimetry and Clearance Kinetics Parameters for ^{225}Ac-DOTA-MC1RL in Non–Tumor-Bearing BALB/c Mice

Parameter	Blood	Brain	Heart	Intestine	Kidney	Liver	Lung	Muscle	Skin	Spleen
^{225}Ac										
Initial activity/organ (kBq)	ND	0.0065	0.0161	1.9113	0.7647	7.6597	0.0512	0.0044	0.0483	0.0426
Effective decay rate constant (h^{-1})	ND	0.0070	0.0030	0.0060	0.0060	0.0040	0.0030	0.0030	0.0050	0.0030
Effective decay half-life (d)	ND	4.1259	9.6270	4.8135	4.8135	7.2203	9.6270	9.6270	5.7762	9.6270
Accumulated activity/organ (kBq × h)	ND	0.7621	3.8089	260.3419	104.1599	1484.6038	12.1242	1.0529	7.7927	10.0784
Absorbed dose/injected activity (Gy/kBq)	ND	0.0002	0.0023	0.0102	0.0300	0.1485	0.0042	0.0004	0.0024	0.0092
^{221}Fr										
Initial activity/organ (kBq)	0.0153	0.0222	0.0349	1.9927	1.3795	8.4464	0.0723	0.0211	0.0705	0.0647
Effective decay rate constant (h^{-1})	0.0010	0.0030	0.0050	0.0070	0.0080	0.0040	0.0020	0.0030	0.0040	0.0040
Effective decay half-life (d)	28.8811	9.6270	5.7762	4.1259	3.6101	7.2203	14.4406	9.6270	7.2203	7.2203
Accumulated activity/organ (kBq × h)	5.6907	5.2622	5.6292	232.2869	139.2517	1637.0734	21.2642	4.9899	13.6614	12.5317
Absorbed dose/injected activity (Gy/kBq)	0.0022	0.0013	0.0037	0.0098	0.0434	0.1770	0.0080	0.0018	0.0045	0.0124
^{217}At										
Initial activity/organ (kBq)	0.0153	0.0222	0.0349	1.9927	1.3795	8.4464	0.0723	0.0211	0.0705	0.0647
Effective decay rate constant (h^{-1})	0.0010	0.0030	0.0050	0.0070	0.0080	0.0040	0.0020	0.0030	0.0040	0.0040
Effective decay half-life (d)	28.8811	9.6270	5.7762	4.1259	3.6101	7.2203	14.4406	9.6270	7.2203	7.2203
Accumulated activity/organ (kBq × h)	5.6907	5.2622	5.6292	232.2869	139.2517	1637.0734	21.2642	4.9899	13.6614	12.5317
Absorbed dose/injected activity (Gy/kBq)	0.0025	0.0014	0.0042	0.0110	0.0486	0.1983	0.0090	0.0021	0.0050	0.0139
^{213}Bi										
Initial activity/organ (kBq)	0.0236	0.0195	0.0309	1.8886	1.0318	6.5122	0.0717	0.0152	0.0627	0.0511
Effective decay rate constant (h^{-1})	0.0010	0.0010	0.0020	0.0050	0.0040	0.0040	0.0020	0.0020	0.0030	0.0030
Effective decay half-life (d)	28.8811	28.881	14.4406	5.7762	7.2203	7.2203	14.4406	14.4406	9.6270	9.6270
Accumulated activity/organ (kBq × h)	8.7917	7.2573	9.0914	304.6111	199.9839	1262.1858	21.0948	4.4603	14.8376	12.1064
Absorbed dose/injected activity (Gy/kBq)	0.0001	0.0000	0.0001	0.0002	0.0012	0.0025	0.0001	0.0000	0.0001	0.0002
^{213}Po										
Initial activity/organ (kBq)	0.0236	0.0195	0.0309	1.8886	1.0318	6.5122	0.0717	0.0152	0.0627	0.0511
Effective decay rate constant (h^{-1})	0.0010	0.0010	0.0020	0.0050	0.0040	0.0040	0.0020	0.0020	0.0030	0.0030
Effective decay half-life (d)	28.8811	28.881	14.4406	5.7762	7.2203	7.2203	14.4406	14.4406	9.6270	9.6270
Accumulated activity/organ (kBq × h)	8.7917	7.2573	9.0914	304.6111	199.9839	1262.1858	21.0948	4.4603	14.8376	12.1064
Absorbed dose/injected activity (Gy/kBq)	0.0044	0.0023	0.0079	0.0168	0.0811	0.1778	0.0103	0.0021	0.0063	0.0156
Total absorbed dose/injected activity (Gy/kBq)	0.0092	0.0053	0.0183	0.0481	0.2042	0.7042	0.0317	0.0064	0.0182	0.0512

ND = not detected.

and ^{213}Bi, respectively. The total absorbed α-particle dose was calculated from the summation of doses from ^{225}Ac, ^{221}Fr, ^{217}At, ^{213}Bi, and ^{213}Po.

Antitumor Efficacy

Tumor-bearing mice (n = 11/group) were injected with activities of ^{225}Ac-DOTA-MC1RL or ^{225}Ac-DOTA-SP, cold lanthanum-DOTA-MC1RL, or saline solution (0.9%, Cardinal Pharmaceuticals). Surpassing a 2,000 mm^3 tumor volume was the experimental endpoint unless clinical endpoints, such as 20% weight loss, tumor ulceration, hunched back, lack of grooming, or lethargy, were observed. Metastasis formation was identified by necropsy.

Statistical Analysis

The t test was used for the MTD study. The following analyses were used for comparison of the efficacy study groups: Kaplan–Meier for time to endpoint, a mixed-model analysis for tumor growth change, a paired Wilcoxon signed-rank test for initial decrease in tumor volume, a Fisher exact test with corrections for multiple testing using the Holm stepdown method for metastasis burden, and a nonparametric Kruskal–Wallis test for immunohistochemistry staining.

RESULTS

Synthesis and Characterization of Parent Compound and Lanthanide Chelates

The unmetallated DOTA-MC1RL was synthesized and, since there are no nonradioactive isotopes of actinium, the analogous lanthanum-DOTA-MC1RL chelate was prepared for use as a nonradioactive control (Supplemental Figs. 4–8) (*23,29*). Both DOTA-MC1RL and lanthanum-DOTA-MC1RL had high binding affinity for human MC1R, 0.24 ± 0.20 and 0.23 ± 0.18 nM inhibition constants, respectively (Supplemental Fig. 9A). The binding affinity of europium-DTPA-MC1RL to human MC1R was determined to be a 4.4 ± 2.3 nM dissociation constant (Supplemental Fig. 9B). Lower, 1.3 μM, dissociation constant affinity was observed for europium-DTPA-MC1RL binding to murine MC1R (Supplemental Fig. 9C). The scrambled peptide controls, lanthanum-DOTA-SP and europium-DOTA-SP, did not bind (Supplemental Figs. 9D and 9E).

TABLE 3
Radiation Dosimetry and Clearance Kinetics for ^{225}Ac-DOTA-MC1RL in SCID Mice Bearing MEL270 Tumors

Parameter	Blood	Bone	Brain	Heart	Intestine	Kidney	Liver	Lung	Muscle	Skin	Spleen	Tumor
^{225}Ac												
Initial activity/organ (kBq)	0.0010	0.0172	0.0031	0.0151	0.3026	0.6417	4.8193	0.0265	0.0042	0.0242	0.0228	0.0518
Effective decay rate constant (h^{-1})	0.0010	0.0030	0.0020	0.0050	0.0130	0.0050	0.0060	0.0050	0.0020	0.0020	0.0040	0.0080
Effective decay half-life (d)	28.8811	9.6270	14.4406	5.7762	2.2216	5.7762	4.8135	5.7762	14.4406	14.4406	7.2203	3.6101
Accumulated activity/organ (kBq × h)	0.2726	3.2443	0.6873	2.1154	16.7417	89.9040	588.513	3.7089	0.9236	5.3441	3.6979	4.9055
Absorbed dose/injected activity (Gy/kBq)	0.0001	0.0041	0.0003	0.0020	0.0012	0.0273	0.0662	0.0025	0.0007	0.0010	0.0107	0.0045
^{221}Fr												
Initial activity/organ (kBq)	0.0036	0.0185	0.0059	0.0192	0.2655	0.6167	4.4828	0.0495	0.0071	0.0362	0.0257	0.0806
Effective decay rate constant (h^{-1})	0.0017	0.0030	0.0010	0.0030	0.0090	0.0040	0.0060	0.0040	0.0020	0.0020	0.0010	0.0070
Effective decay half-life (d)	16.9889	9.6270	28.8811	9.6270	3.2090	7.2203	4.8135	7.2203	14.4406	14.4406	28.881	4.1259
Accumulated activity/organ (kBq × h)	0.8370	3.4960	1.5396	3.6259	22.3311	99.8475	547.425	8.0162	1.5699	8.0166	6.7303	8.6407
Absorbed dose/injected activity (Gy/kBq)	0.0002	0.0047	0.0007	0.0037	0.0017	0.0328	0.0666	0.0058	0.0014	0.0017	0.0211	0.0086
^{217}At												
Initial activity/organ (kBq)	0.0036	0.0185	0.0059	0.0192	0.2655	0.6167	4.4828	0.0495	0.0071	0.0362	0.0257	0.0806
Effective decay rate constant (h^{-1})	0.0017	0.0030	0.0010	0.0030	0.0090	0.0040	0.0060	0.0040	0.0020	0.0020	0.0010	0.0070
Effective decay half-life (d)	16.9889	9.6270	28.8811	9.6270	3.2090	7.2203	4.8135	7.2203	14.4406	14.4406	28.881	4.1259
Accumulated activity/organ (kBq × h)	0.8370	3.4960	1.5396	3.6259	22.3311	99.8475	547.425	8.0162	1.5699	8.0166	6.7303	8.6407
Absorbed dose/injected activity (Gy/kBq)	0.0003	0.0053	0.0007	0.0041	0.0019	0.0367	0.0746	0.0065	0.0015	0.0019	0.0236	0.0097
^{213}Bi												
Initial activity/organ (kBq)	0.0016	0.0133	0.0027	0.0082	0.2160	0.5664	3.9089	0.0175	0.0017	0.0240	0.0131	0.0381
Effective decay rate constant (h^{-1})	0.0013	0.0020	0.0007	0.0040	0.0100	0.0040	0.0060	0.0060	0.0020	0.0050	0.0030	0.0060
Effective decay half-life (d)	22.2163	14.4406	41.2588	7.2203	2.8881	7.2203	4.8135	4.8135	14.4406	5.7762	9.6270	4.8135
Accumulated activity/organ (kBq × h)	0.4096	2.9358	0.7531	1.3342	16.2384	91.7024	477.346	2.1354	0.3859	3.3617	2.4736	4.6565
Absorbed dose/injected activity (Gy/kBq)	2.20E-06	7.39E-05	5.96E-06	2.51E-05	2.32E-05	5.61E-04	1.08E-03	2.88E-05	6.19E-06	1.32E-05	1.44E-04	8.68E-05
^{213}Po												
Initial activity/organ (kBq)	0.0016	0.0133	0.0027	0.0082	0.2160	0.5664	3.9089	0.0175	0.0017	0.0240	0.0131	0.0381
Effective decay rate constant (h^{-1})	0.0013	0.0020	0.0007	0.0040	0.0100	0.0040	0.0060	0.0060	0.0020	0.0050	0.0030	0.0060
Effective decay half-life (d)	22.2163	14.4406	41.2588	7.2203	2.8881	7.2203	4.8135	4.8135	14.4406	5.7762	9.6270	4.8135
Accumulated activity/organ (kBq × h)	0.4096	2.9358	0.7531	1.3342	16.2384	91.7024	477.346	2.1354	0.3859	3.3617	2.4736	4.6565
Absorbed dose/injected activity (Gy/kBq)	0.0002	0.0052	0.0004	0.0018	0.0016	0.0392	0.0756	0.0020	0.0004	0.0009	0.0101	0.0061
Total absorbed dose/injected activity (Gy/kBq)	0.0007	0.0193	0.0021	0.0115	0.0065	0.1366	0.2842	0.0168	0.0040	0.0056	0.0656	0.0290

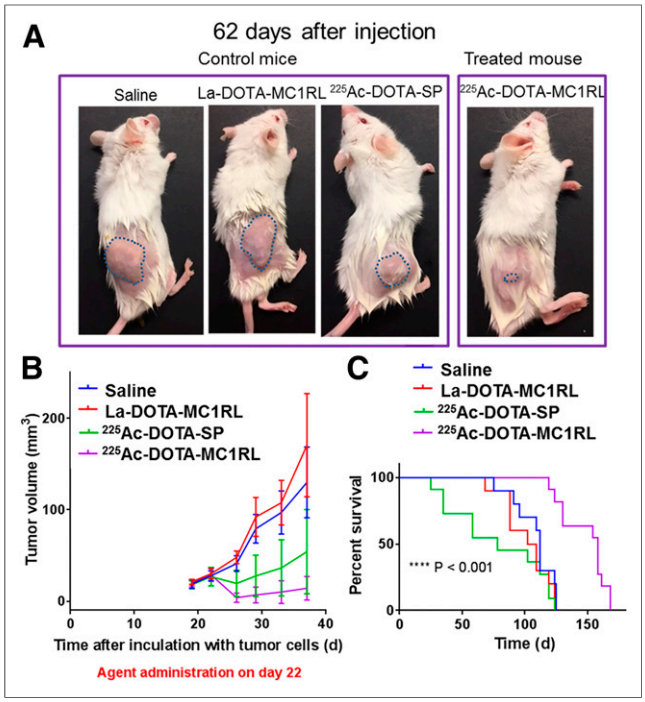

FIGURE 6. Efficacy study in mice bearing MEL270 tumors: representative images of tumors (outlined) (A); initial tumor growth volumes (B); and Kaplan–Meier plots (C).

Radiosynthesis and Characterization of ^{225}Ac Radiopharmaceutical

Radiochemical purity of 99.8% and specific activity of 181.3 ± 92.5 kBq/μg and 140.6 ± 55.5 kBq/μg for ^{225}Ac-DOTA-MC1RL and ^{225}Ac-DOTA-SP, respectively, were observed (Supplemental Fig. 10). In vitro serum stability was high, with 90% intact after 10 d (Table 1).

MC1R Expression on Uveal Melanoma Cell Lines and Xenograft Tumors

MC1R messenger RNA and protein expression were confirmed in a set of uveal melanoma cell lines (Supplemental Fig. 11). Only MEL270, OMM2.3, and OMM1 cells carry the GNAQ or GNA11 mutations found in nearly all uveal melanomas (*30*). The MEL270 and OMM1 cells formed tumors in immunocompromised mice, and all xenografts had high and uniform MC1R protein expression.

Receptor Number for Tumor Cell Lines

MEL270 cells were selected for the in vivo studies, and it was determined that MEL270 cells have 410,000 receptors per cell (Supplemental Fig. 12), which is a higher level of endogenous expression than that of the engineered A375/MC1R cells, which have 75,000 receptors per cell (*12*). The parental A375 melanoma cell line has extremely low expression, at 400 ± 93 MC1Rs per cell (*31*).

In Vitro MC1R-Specific Cytotoxicity

Cytotoxicity assays were performed with the goal of demonstrating target-specific cytotoxicity. Assay conditions were not optimized to demonstrate maximal toxicity. Significantly reduced proliferation ($P < 0.0001$) was observed in uveal melanoma cells and the engineered A375/MC1R cells treated with ^{225}Ac-DOTA-MC1RL relative to the untargeted ^{225}Ac-DOTA-SP or phosphate-buffered saline controls (Supplemental Fig. 2). All cell lines also had a significant ($P < 0.001$) response to incubation with ^{225}Ac-DOTA-SP relative to phosphate-buffered saline. However, there was no significant difference in A375 cell proliferation (extremely low MC1R) when treated with either the targeted or the untargeted radiopharmaceutical. These results demonstrate MC1R-specific cytotoxicity. Assay replicates yielded comparable results.

MTD

The MTD was evaluated in immune-competent non–tumor-bearing BALB/c mice (n = 5/cohort). Cohorts received a single intravenous injection of ^{225}Ac-DOTA-MC1RL over the range of 0–148 kBq in the syringe. At completion of the study (>11 ^{225}Ac half-lives, 118 d after injection), serum and tissues (adipose, bone, cecum, colon, duoden, esophageal, heart, ileum, kidney, liver, lung, lymph nodes, muscle, pancreas, small intestine, spleen, and stomach) were collected for histology and then examined in a masked manner by a veterinary pathologist to assess radiation-induced tissue damage. No remarkable damage was observed in any of the tissues (Supplemental Figs. 13–16). For example, the control kidneys had minimal multifocal interstitial fibrosis and minimal medullary protein in tubules, which were both considered to be incidental findings. The incidental minimal medullary protein was also found in some kidneys from the groups that received treatment activities, but each treatment group also included kidneys that were within normal limits for all types of damage. The cortex of one kidney from the group with the highest administered activity had a focal extracellular cortical hyaline substance that was healing and was considered to be an incidental finding (Supplemental Fig. 14D). Blood urea nitrogen and creatinine, which are important indicators of renal function, were also determined and were not significantly elevated among the groups (Figs. 2B and 2C). All animals had gained weight by the end of the study, albeit less weight was gained by animals at the highest dose level than in the lowest (Fig. 2A).

Pharmacokinetics and Biodistribution

In rats, ^{225}Ac-DOTA-MC1RL rapidly cleared (<15 min after injection) from blood circulation (Fig. 3). After administration to non–tumor-bearing BALB/c mice, ^{225}Ac activities were observed primarily in clearance tissues. At 24 h after injection of ^{225}Ac-DOTA-MC1RL, the liver, kidneys, spleen, and intestine had 21.2 ± 2.8, 6.9 ± 0.9, 2.9 ± 0.8, and 2.9 ± 2.0 %IA/g, whereas negligible activity was observed in the other tissues measured. Activity had largely cleared from the tissues at 1–3 wk (Fig. 4A). For tumor-bearing animals, activity was retained in MC1R-positive tumors, that is, MEL270 (Fig. 4B) and A375/MC1R tumors (Fig. 5A), which had 3.6 ± 1.2 and 2.8 ± 0.8 %IA/g, respectively, compared with the nominal 0.30 ± 0.1 %IA/g in the MC1R-negative A375 tumors at 24 h after injection. The clearance tissues in tumor-bearing animals had lower activities than in non–tumor-bearing mice: for example, 14.4 ± 1.7 %IA/g in the livers of MEL270 tumor-bearing mice at 24 h (Fig. 4B), compared with the 21.2 ± 2.8 %IA/g in the non–tumor-bearing mice (Fig. 4A). The ^{225}Ac-DOTA-SP tumor distribution in the bilateral A357 and A375/MC1R model was also determined, and as expected, uptake was minimal and did not differ between the positive and negative A375 tumors (Fig. 5B). The distribution of ^{221}Fr and ^{213}Bi was also determined (Figs. 4 and 5). However, since ^{225}Ac and daughters are at secular equilibrium by 24 h after injection and the ^{221}Fr and ^{213}Bi atoms

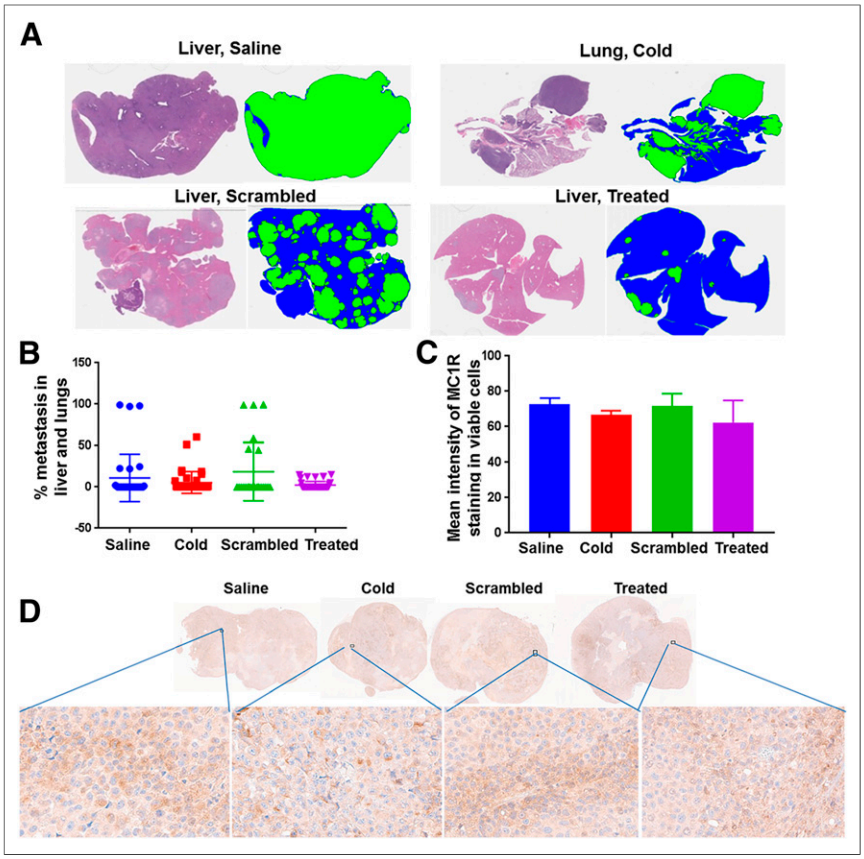

FIGURE 7. Metastasis study in MEL270 uveal melanoma mouse model and MC1R expression in tumors reaching endpoints from each treatment group: representative hematoxylin and eosin staining and corresponding threshold segmentations of sections containing liver and lung metastases (cold = lanthanum-DOTA-MC1RL; scrambled = untargeted; treated = ^{225}Ac-DOTA-MC1RL; blue = normal tissue; green = metastasis) (A); quantified metastasis burden (B); graph (C) and sections (D) for MC1R immunohistochemistry staining of MEL270 tumors after reaching endpoints.

present during injection will be mostly decayed, the ^{221}Fr and ^{213}Bi detected in the samples are from decay of the ^{225}Ac taken into the tissues.

Radiation Dosimetry

Biodistribution data were fitted (Supplemental Fig. 17), and clearance kinetics, tissue biologic half-life, accumulated activity, and absorbed dose/injected activity (Gy/kBq) were estimated for each radionuclide in each tissue for non–tumor-bearing and MEL270 tumor-bearing mice (Tables 2 and 3). The effective decay half-lives calculated for ^{225}Ac in tissues—for example, 7.2 d in liver—were shorter than the radiodecay half-life of ^{225}Ac (10 d), indicating biologic clearance. The calculated total absorbed dose per injected activity (Gy/kBq) for ^{225}Ac-DOTA-MC1RL was minimal in all tissues except clearance organs and positive tumor. Since the positive tumors shrank rapidly in response to the treatment and the total absorbed doses were extrapolated from data collected over a 2-wk period, the dose values for the tumors are likely subdued relative to the clearance organs, which did not have appreciable cellular toxicity at the administered activities. The total absorbed dose in the liver was generally lower in mice with tumors than in nontumor mice: for example, 0.284 and 0.704 Gy/kBq, respectively.

Antitumor Efficacy

SCID mice bearing MEL270 tumors (124 ± 36 mm^3 pretreatment tumor volumes) were injected with a single administration of ^{225}Ac-DOTA-MC1RL (92.5 ± 9.3 kBq), ^{225}Ac-DOTA-SP (99.9 ± 9.9 kBq), lanthanum-DOTA-MC1RL (1 pmol/mouse), or saline. Representative images show much smaller tumors in treated mice than in controls (Fig. 6A), and tumor volumes decreased immediately after treatment relative to controls ($P = 0.001$) before eventual regrowth (Fig. 6B). Treated mice had a significantly delayed time to experimental or clinical endpoint ($P < 0.001$), with a median survival of 148 d, compared with the median survival of control groups (79–108 d), and differences among the controls were not significant (Fig. 6C). In this study, some animals were euthanized because of reaching clinical endpoints instead of the experimental endpoint (Supplemental Table 1). Some of the animals that reached clinical endpoints had metastases in the liver or lungs, and metastasis burden was significantly lower in the ^{225}Ac-DOTA-MC1RL treated group than in the controls ($P = 0.024$) (Figs. 7A and 7B). Mice bearing A375/MC1R tumors (240 ± 110 mm^3 pretreatment volume) were also injected with either sterile saline, lanthanum-DOTA-MC1RL, 107.3 ± 11.1 kBq of ^{225}Ac-DOTA-SP, or 59.2 ± 5.9 kBq of ^{225}Ac-DOTA-MC1RL, and significant decreases in tumor volume ($P = 0.005$) and tumor growth delay ($P < 0.0001$) were observed. Some tumors that disappeared did not recur, and those mice lived their natural life span (Supplemental Figs. 18A–18C). After tumors reached an endpoint, MC1R staining was quantified, and the level of MC1R expression was not significantly different in treated tumors that responded by shrinking before regrowth relative to control tumors ($P = 0.60$ for MEL270 and $P = 0.82$ for A375/MC1R) (Figs. 7C and 7D; Supplemental Fig. 18D).

DISCUSSION

We have developed and evaluated a novel MC1R-targeted radiopharmaceutical, ^{225}Ac-DOTA-MC1RL, for TAT of metastatic uveal melanoma. The choice of using a peptide-targeting ligand is reinforced by the recent preclinical and clinical successes of TAT radiopeptides (*14,15,32–34*). Another group has also reported the development of a peptide-based TAT, ^{212}Pb-CCMSH, that is targeted to melanocortin receptors for treatment of melanoma (*35*). However, ^{212}Pb-CCMSH was associated with renal toxicity. This is likely due to the use of an α-MSH derivative–targeting ligand, as α-MSH has specificity for multiple melanocortin receptor isoforms, including MC5R, which is expressed in the human kidney and lungs (*6*). The MC1RL-targeting moiety used in the current work has specificity for the MC1R isoform (*13*), greatly reducing the potential for renal toxicity. Another advantage of ^{225}Ac-DOTA-MC1RL over the ^{212}Pb-TAT agent is that ^{225}Ac has greater cell-killing potential through

generation of 4 α-particle emissions per radionuclide, compared with the single α-emission of ^{212}Pb, in their relative decay chains (*35,36*).

^{225}Ac-DOTA-MC1RL has high affinity for MC1R, high radiochemistry yield and purity, high biostability, and MC1R-specific cytotoxicity in vitro. In vivo studies demonstrated low toxicity, rapid blood clearance, and uptake into MC1R-positive tumors and clearance organs. Biodistribution studies demonstrated that ^{225}Ac remains in the compartments where ^{225}Ac-DOTA-MC1RL was initially distributed, that is, tumors and clearance organs, and the corresponding clearance kinetics parameters and radiation dose delivered by all α-particle–emitting radioisotopes in the decay chain were calculated. Considering the 10-d half-life of ^{225}Ac, most of the administered ^{225}Ac-DOTA-MC1RL will have either been taken into tumor cells (*7*) or cleared from the blood before decay. Hence, ^{225}Ac-DOTA-MC1RL likely functions as an in vivo α-particle generator, concentrating α-emissions in the target tumor tissues, with limited translocation of daughter isotopes (*32*). This is consistent with the recent observations of efficacy with low toxicity observed for an ^{225}Ac-PSMA–targeting small-molecule conjugate (*37*).

In vivo efficacy studies demonstrated significant tumor and metastasis growth delay and prolonged survival in human uveal and cutaneous melanoma xenograft models in mice after a single treatment of ^{225}Ac-DOTA-MC1RL, including some cures. Tumors that shrank and regrew after treatment had the same MC1R expression levels as controls, suggesting that multiple treatment regimens would increase efficacy.

CONCLUSION

We have developed and evaluated a novel MC1R-targeted radiopharmaceutical for TAT of metastatic uveal melanoma. In vivo studies demonstrated low toxicity, rapid blood clearance, uptake into MC1R-positive tumors and clearance organs, significant tumor and metastasis growth delay, and prolonged survival in human uveal melanoma xenograft models in mice after a single treatment of ^{225}Ac-DOTA-MC1RL. This novel radiopharmaceutical has strong potential to benefit patients with metastatic uveal melanoma, which has had no significant improvement in treatment in the last 20 y.

DISCLOSURE

Funding was provided by a Miles for Moffitt Milestone Award (principal investigator, David Morse), the Moffitt Imaging and Technology Center of Excellence, an NIH/NCI–Moffitt Skin Cancer SPORE (P50CA168536-03) Career Enhancement Program award (principal investigator, David Morse), an NIH/NCI SBIR Phase 1 Contract to Modulation Therapeutics, Inc. (principal investigator, Narges Tafreshi), and a Melanoma Research Alliance Team Science Award (principal investigator, David Morse). This work was supported by the Analytic Microscopy, Bioinformatics and Biostatistics, Molecular Genomics, Proteomics, Small Animal Imaging Laboratory, and Tissue Core Facilities at the H. Lee Moffitt Cancer Center and Research Institute, an NCI-designated Comprehensive Cancer Center (P30-CA076292). David Morse, Thaddeus Wadas, Mark McLaughlin, HyunJoo Kil, and Narges Tafreshi are coinventors on a pending patent application. The pending patent has been licensed to Modulation Therapeutics Inc., and Mark McLaughlin is a cofounder of that company. No other potential conflict of interest relevant to this article was reported.

ACKNOWLEDGMENTS

Animal studies were conducted in the Moffitt Barrier Vivarium that is administered by the University of South Florida Comparative Medicine Department. The ^{225}Ac isotope used in this research was supplied by the U.S. Department of Energy Office of Science by the Isotope Program in the Office of Nuclear Physics.

REFERENCES

1. Chattopadhyay C, Kim DW, Gombos DS, et al. Uveal melanoma: from diagnosis to treatment and the science in between. *Cancer.* 2016;122:2299–2312.
2. Krantz BA, Dave N, Komatsubara KM, Marr BP, Carvajal RD. Uveal melanoma: epidemiology, etiology, and treatment of primary disease. *Clin Ophthalmol.* 2017;11:279–289.
3. Komatsubara KM, Carvajal RD. Immunotherapy for the treatment of uveal melanoma: current status and emerging therapies. *Curr Oncol Rep.* 2017;19:45.
4. López MN, Pereda C, Ramirez M, et al. Melanocortin 1 receptor is expressed by uveal malignant melanoma and can be considered a new target for diagnosis and immunotherapy. *Invest Ophthalmol Vis Sci.* 2007;48:1219–1227.
5. Yang Y. Structure, function and regulation of the melanocortin receptors. *Eur J Pharmacol.* 2011;660:125–130.
6. Chhajlani V. Distribution of cDNA for melanocortin receptor subtypes in human tissues. *Biochem Mol Biol Int.* 1996;38:73–80.
7. Tafreshi NK, Silva A, Estrella VC, et al. In vivo and in silico pharmacokinetics and biodistribution of a melanocortin receptor 1 targeted agent in preclinical models of melanoma. *Mol Pharm.* 2013;10:3175–3185.
8. Ainger SA, Jagirdar K, Lee KJ, Soyer HP, Sturm RA. Skin pigmentation genetics for the clinic. *Dermatology.* 2017;233:1–15.
9. Ezzedine K, Eleftheriadou V, Whitton M, van Geel N. Vitiligo. *Lancet.* 2015;386:74–84.
10. Salazar-Onfray F, Lopez M, Lundqvist A, et al. Tissue distribution and differential expression of melanocortin 1 receptor, a malignant melanoma marker. *Br J Cancer.* 2002;87:414–422.
11. Tagliabue E, Fargnoli MC, Gandini S, et al. MC1R gene variants and non-melanoma skin cancer: a pooled-analysis from the M-SKIP project. *Br J Cancer.* 2015;113:354–363.
12. Tafreshi NK, Huang X, Moberg VE, et al. Synthesis and characterization of a melanoma-targeted fluorescence imaging probe by conjugation of a melanocortin 1 receptor (MC1R) specific ligand. *Bioconjug Chem.* 2012;23:2451–2459.
13. Barkey NM, Tafreshi NK, Josan JS, et al. Development of melanoma-targeted polymer micelles by conjugation of a melanocortin 1 receptor (MC1R) specific ligand. *J Med Chem.* 2011;54:8078–8084.
14. Morgenstern A, Apostolidis C, Kratochwil C, Sathekge M, Krolicki L, Bruchertseifer F. An overview of targeted alpha therapy with 225actinium and 213bismuth. *Curr Radiopharm.* 2018;11:200–208.
15. Makvandi M, Dupis E, Engle JW, et al. Alpha-emitters and targeted alpha therapy in oncology: from basic science to clinical investigations. *Target Oncol.* 2018;13:189–203.
16. Baidoo KE, Yong K, Brechbiel MW. Molecular pathways: targeted alpha-particle radiation therapy. *Clin Cancer Res.* 2013;19:530–537.
17. Deblonde GJ, Abergel RJ. Active actinium. *Nat Chem.* 2016;8:1084.
18. Ma D, McDevitt MR, Finn RD, Scheinberg DA. Breakthrough of ^{225}Ac and its radionuclide daughters from an ^{225}Ac/^{213}Bi generator: development of new methods, quantitative characterization, and implications for clinical use. *Appl Radiat Isot.* 2001;55:667–678.
19. Josan JS, De Silva CR, Yoo B, et al. Fluorescent and lanthanide labeling for ligand screens, assays, and imaging. *Methods Mol Biol.* 2011;716:89–126.
20. Handl HL, Vagner J, Yamamura HI, Hruby VJ, Gillies RJ. Lanthanide-based time-resolved fluorescence of in cyto ligand-receptor interactions. *Anal Biochem.* 2004;330:242–250.
21. Reid Y, Storts D, Riss T, Minor L. Authentication of human cell lines by STR DNA profiling analysis. In: Sittampalam GS, Coussens NP, Brimacombe K, et al. *Assay Guidance Manual.* Bethesda, MD: Eli Lily & Company and the National Center for Advancing Translational Science; 2004:1–21.
22. Bonardi ML, de Goeij JJM. How do we ascertain specific activities in no-carrier-added radionuclide preparations? *J Radioanal Nucl Chem.* 2005;263:87–92.

23. Pandya DN, Hantgan R, Budzevich MM, et al. Preliminary therapy evaluation of ^{225}Ac-DOTA-c(RGDyK) demonstrates that Cerenkov radiation derived from ^{225}Ac daughter decay can be detected by optical imaging for in vivo tumor visualization. *Theranostics.* 2016;6:698–709.
24. Apostolidis C, Molinet R, Rasmussen G, Morgenstern A. Production of Ac-225 from Th-229 for targeted alpha therapy. *Anal Chem.* 2005;77:6288–6291.
25. Robertson AKH, Ramogida CF, Rodriguez-Rodriguez C, et al. Multi-isotope SPECT imaging of the ^{225}Ac decay chain: feasibility studies. *Phys Med Biol.* 2017;62:4406–4420.
26. Song H, Hobbs RF, Vajravelu R, et al. Radioimmunotherapy of breast cancer metastases with alpha-particle emitter ^{225}Ac: comparing efficacy with ^{213}Bi and ^{90}Y. *Cancer Res.* 2009;69:8941–8948.
27. Bolch WE, Eckerman KF, Sgouros G, Thomas SR. MIRD pamphlet no. 21: a generalized schema for radiopharmaceutical dosimetry–standardization of nomenclature. *J Nucl Med.* 2009;50:477–484.
28. Kratochwil C, Bruchertseifer F, Rathke H, et al. Targeted alpha therapy of mCRPC with ^{225}actinium-PSMA-617: dosimetry estimate and empirical dose finding. *J Nucl Med.* 2017;58:1624–1631.
29. Thiele NA, Wilson JJ. Actinium-225 for targeted alpha therapy: coordination chemistry and current chelation approaches. *Cancer Biother Radiopharm.* 2018;33:336–348.
30. Griewank KG, Yu X, Khalili J, et al. Genetic and molecular characterization of uveal melanoma cell lines. *Pigment Cell Melanoma Res.* 2012;25:182–187.
31. Cheng Z, Xiong Z, Subbarayan M, Chen X, Gambhir SS. ^{64}Cu-labeled alpha-melanocyte-stimulating hormone analog for microPET imaging of melanocortin 1 receptor expression. *Bioconjug Chem.* 2007;18:765–772.
32. Miederer M, Henriksen G, Alke A, et al. Preclinical evaluation of the alpha-particle generator nuclide ^{225}Ac for somatostatin receptor radiotherapy of neuroendocrine tumors. *Clin Cancer Res.* 2008;14:3555–3561.
33. Nayak TK, Norenberg JP, Anderson TL, Prossnitz ER, Stabin MG, Atcher RW. Somatostatin-receptor-targeted alpha-emitting ^{213}Bi is therapeutically more effective than beta(−)-emitting ^{177}Lu in human pancreatic adenocarcinoma cells. *Nucl Med Biol.* 2007;34:185–193.
34. Drecoll E, Gaertner FC, Miederer M, et al. Treatment of peritoneal carcinomatosis by targeted delivery of the radio-labeled tumor homing peptide bi-DTPA-[F3]2 into the nucleus of tumor cells. *PLoS One.* 2009; 4:e5715.
35. Miao Y, Hylarides M, Fisher DR, et al. Melanoma therapy via peptide-targeted α-radiation. *Clin Cancer Res.* 2005;11:5616–5621.
36. McDevitt MR, Ma D, Lai LT, et al. Tumor therapy with targeted atomic nanogenerators. *Science.* 2001;294:1537–1540.
37. Kratochwil C, Bruchertseifer F, Rathke H, et al. Targeted alpha-therapy of metastatic castration-resistant prostate cancer with ^{225}Ac-PSMA-617: swimmer-plot analysis suggests efficacy regarding duration of tumor control. *J Nucl Med.* 2018;59:795–802.